

Received June 26, 2018; Reviewed; Accepted October 2, 2018

## Study on the application of elliptic cross-section matrices for axial high gradient magnetic separation: key considerations for optimization

Xiayu Zheng<sup>1,2</sup>, Yuhua Wang<sup>1,2</sup>, Dongfang Lu<sup>1,2</sup>, Xudong Li<sup>1,2</sup>

<sup>1</sup> School of Minerals Processing & Bioengineering, Central South University, Changsha 410083, China

<sup>2</sup> Key Laboratory of Hunan Province for Clean and Efficient Utilization of Strategic Calcium-containing Mineral Resources, Central South University, Changsha 410083, China

Corresponding authors: wangyh@csu.edu.cn (Yuhua Wang), 82559428@qq.com (Dongfang Lu)

**Abstract:** To reveal the key optimization considerations for the application of elliptic cross-section matrices in axial high gradient magnetic separation (HGMS), the performance of circular and elliptic matrices was investigated experimentally and theoretically, providing that the short axis of elliptic matrix was equal to the diameter of circular matrix. Three schemes were adopted to investigate the performance matrices with ratio of long axis to short axis  $\lambda$  of 1 (circular matrix), 1.6 and 2. Under the same matrix unit number, hematite recovery of elliptic matrices could be 5~20% higher than that of circular matrices. For the case that the separation space was fully filled under the same matrix unit spacing, elliptic matrices showed higher and lower hematite recovery in low and relatively high magnetic field. The particle capture cross section area of elliptic matrix could be 1.4~1.8 times larger than that of circular matrix. Analyses with particle capture models showed that higher hematite recovery was ascribed to the larger particle capture cross section of the elliptic matrices and overlapping of the capture cross section was responsible for the lower hematite recovery of elliptic matrices in relatively high magnetic field. For substitution of circular matrices with elliptic matrices in axial HGMS, overlapping of capture cross section of target particles should be taken into consideration.

**Keywords:** elliptic matrices, expanded capture models, capture cross section, overlapping

### 1. Introduction

High gradient magnetic separation (HGMS) is effective in recovering fine weakly magnetic materials from slurry or suspension and has been witnessed widespread applications in many scientific and industrial fields such as mineral processing (Singh et al., 2013; Li et al., 2018; Tripathy and Suresh, 2017a; Singh et al., 2015; Chen, 2011), water purification (Mariani et al., 2010; Toh et al., 2012), biology entity separation (Chen et al., 2008) and protein separation (Lindner et al., 2013; Pasteur et al., 2014). Magnetic matrices dehomogenize the magnetic field, inducing large magnetic field gradient and providing capture sites for paramagnetic particles. As the widespread applications of HGMS in a variety of fields, theory construction on HGMS also attracted much attention from scientific researchers. Watson calculated the magnetic field around the circular cylinders and derived the particle motion equations in longitudinal and transversal configurations (Watson, 1973; Watson, 1975). Briss and Uchiyama derived the particle motion equations in axial configuration of HGMS (Briss et al., 1976; Uchiyama et al., 1976). Some other researchers also studied the particle capture in HGMS for some specific conditions (Abbasov et al., 1999; Lacoba and Rezlescu, 1998; Kanok and Mayuree, 2013; abbasov et al., 2016). With the particle capture models, we investigated the particle capture of fine weakly magnetic minerals in HGMS, for both the mineral monomers and intergrowths (Zheng et al., 2015a; Zheng et al., 2015b; Zheng et al., 2017a). However, nearly all these models were established only for matrices saturated by the applied magnetic field.

There are many factors influencing the separation performance in HGMS (Zheng et al., 2015a; Tripathy et al., 2017b). The matrix is the key component of the HGMS system and has significant influence on separation performance of HGMS. The most commonly used matrices in HGMS is cylinders of high magnetic susceptibility. The matrix cross-section significantly affects the matrix's magnetic characteristics and consequently the matrix's performance in HGMS (Li Et al., 2007; Nakai et al., 2010; Kim et al., 2013). We had previously investigated the performance of elliptic cross-section matrices in HGMS and established the particle capture models of elliptic cross-section matrices (Zheng et al., 2016a; Zheng et al., 2016b; Zheng et al., 2016c; Zheng et al., 2017b). Additionally, based on experimental results, we expanded the particle capture models of circular and elliptic matrices (circular and elliptic cross-section matrices for short) in HGMS for the case that the matrices were unsaturated by the applied magnetic field (Zheng et al., 2017c; Zheng et al., 2017d). The demarcation of the applied magnetic induction for determining the magnetization state (saturated or unsaturated) of the matrices were also investigated (Wang et al., 2018a; Wang et al., 2018b). The theoretical and experimental results revealed that the elliptic matrices presented better performance than circular matrices, especially when the matrices were unsaturated. For the axial HGMS, we had studied the performance of circular and elliptic matrices under the same matrix cross-section area (Zheng et al., 2017c). Higher hematite recovery could be obtained employing elliptic matrices due to the larger particle capture cross section. However, it should be noted that, for the application of elliptic matrices in HGMS, the case that the elliptic and circular matrices have equal cross-section area is just one scheme, particle capture performance can be further enhanced with elliptic matrices with other shape relationship respect to circular matrices, i.e., more ultra-fine magnetic particles can be recovered under the optimal matrix design. Considering the good magnetic characteristics of elliptic matrices, it is necessary to investigate the performance of elliptic matrices with other shape relationship with respect to circular matrices (ellptic matrices with short axis equal to the diameter of circular matrices or elliptic matrices with long axis equal to the diameter of the circular matrices). More importantly, the role of some influencing factors can not be revealed under the same matrix cross-section area and packing fraction (Zheng et al., 2017c).

In this paper, the performance of circular and elliptic matrices in the axial HGMS was investigated experimentally and theoretically, providing that the short axis of the elliptic matrices was equal to the diameter of circular matrices. The aim of this study is to investigate that in which circumstances the particle capture efficiency of elliptic matrices can be higher than that of the circular matrices and at the same time, to reveal the key factors influencing the difference of particle capture between the two kinds of matrices. It is also expected that the present paper can provide guidance for the design and optimization of elliptic matrices in axial HGMS.

## 2. The expanded particle capture models of circular and elliptic matrices in axial HGMS

### 2.1. Expanded particle capture model of circular matrix

In axial HGMS, the matrix is placed along the direction of the flow and the magnetic field is perpendicular to the matrix axis. As had been mentioned, we established the particle capture model of elliptic matrices in the axial HGMS (Zheng et al., 2016a) and we expanded the particle capture models of circular and elliptic matrices for the case that the matrices were unsaturated by the applied magnetic field (Zheng et al., 2017c). Fig. 1 shows the cross-section of the circular and elliptic matrices. The expanded particle capture model of circular matrix in axial HGMS in the polar coordinate system is as follow:

$$\frac{dr}{dt} = -\frac{4\mu_0\kappa R^2}{9\eta} \left( \frac{A_1 H_0 \cos 2\theta}{r^3} + \frac{A_1^2}{r^5} \right) \quad (1)$$

$$r \frac{d\theta}{dt} = -\frac{4\mu_0\kappa R^2}{9\eta} \frac{A_1 H_0 \sin 2\theta}{r^3} \quad (2)$$

$$\frac{dz}{dt} = V_0 \quad (3)$$

where  $H_0$  is the applied magnetic field,  $\mu_0$  is vacuum permeability,  $\kappa$  is the susceptibility of the particle,  $\eta$  is the fluid viscosity,  $r$  and  $\theta$  are the polar coordinates,  $R$  is the radius of the particle,  $V_0$  is the velocity

of the slurry.  $A_1$  is a coefficient determined by the magnetization state of the matrix. For unsaturated matrices,  $A_1$  is determined by the following equation:

$$A_1 = H_0 d^2 \tag{4}$$

where  $d$  is the radius of the circular matrix. When the matrix is saturated,  $A_1$  is determined by Eq. (5).

$$A_1' = M_s d^2 / (2\mu_0) \tag{5}$$

where  $M_s$  is the saturation magnetization of the matrix.

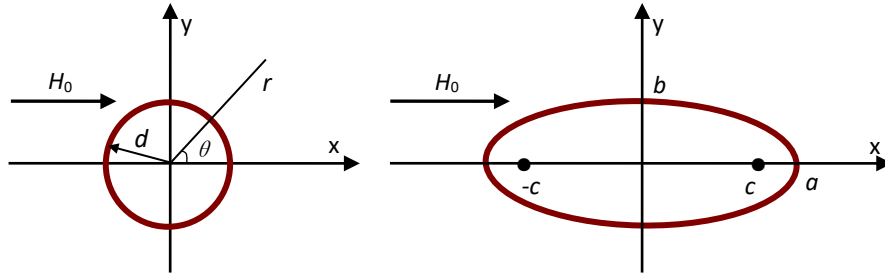


Fig. 1. The cross-section of the circular and elliptic matrices

**2.2. Expanded particle capture model of elliptic matrix**

The cross-section of the elliptic matrix is shown in Fig. 1. The components of the magnetic field around the elliptic matrix in the elliptic coordinate system are as follows (Zheng et al., 2017c):

$$H_v = H_0 \frac{\cos u}{2\sqrt{sh^2v + \sin^2 u}} (e^v - A_2 e^{-v}) \tag{6}$$

$$H_u = -H_0 \frac{\sin u}{2\sqrt{sh^2v + \sin^2 u}} (e^v + A_2 e^{-v}) \tag{7}$$

where  $A_2$  is a coefficient determined by the magnetization state of the elliptic matrix,  $e$  is the napierian base,  $u$  and  $v$  are the coordinates in the elliptic coordinate system,  $u \in [0, 2\pi], v \in [0, +\infty)$ . For unsaturated and saturated matrices,  $A_2$  is determined by Eqs. (8) and (9), respectively.

$$A_2 = -e^{2v_0} \tag{8}$$

$$A_2' = 1 - 2M_s shv_0 chv_0 / (\mu_0 H_0) \tag{9}$$

where  $v_0$  is the coordinate value of the matrix boundary.

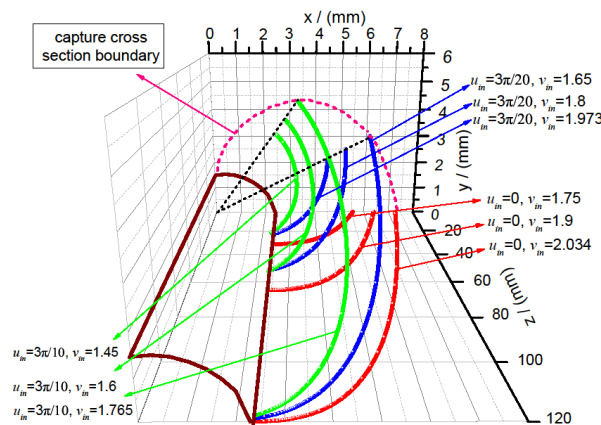


Fig. 2. Particle motion trajectories around the elliptic matrix: half the long and short axes of the matrix were 2.4 mm and 1.5 mm,  $R=25 \mu\text{m}$ ,  $B_0=0.4 \text{ T}$

With the components of the magnetic field, the particle capture equations of the elliptic matrix in axial HGMS can be derived, as shown of Eqs. (10) to (12).

$$c\sqrt{sh^2v + \sin^2 u} \frac{dv}{dt} = V_m \left[ \frac{e^{2v} - A_2^2 e^{-2v}}{4(sh^2v + \sin^2 u)^{3/2}} - \frac{shvchv(e^{2v} + A_2^2 e^{-2v} - 2A_2 \cos 2u)}{4(sh^2v + \sin^2 u)^{5/2}} \right] \quad (10)$$

$$c\sqrt{sh^2v + \sin^2 u} \frac{du}{dt} = V_m \left[ \frac{A_2 \sin 2u}{2(sh^2v + \sin^2 u)^{3/2}} - \frac{\sin 2u(e^{2v} + A_2^2 e^{-2v} - 2A_2 \cos 2u)}{8(sh^2v + \sin^2 u)^{5/2}} \right] \quad (11)$$

$$\frac{dz}{dt} = V_0 \quad (12)$$

where  $V_m = 2\mu_0 k H_0^2 R^2 / (9\eta c)$ ,  $A_2$  is determined by Eqs. (8) and (9) for unsaturated and saturated matrices, respectively. Fig. 2 shows the typical trajectories of magnetic particles around the elliptic matrices calculated basing on the particle motion equations.

### 3. Experimental

#### 3.1. The matrix units and the tailored boxes

In this study, three kinds of matrices were manufactured by the numerical control machines: circular matrices of radius 3mm; elliptic matrices with long and short axes of 4.8 mm and 3 mm; elliptic matrices with long and short axes of 6 mm and 3 mm. Assuming  $\lambda$  was the ratio of the long axis to the short axis of the matrices, the  $\lambda$  for the three kinds of matrices above were 1 (circular matrix), 1.6 and 2, respectively. The length of the matrices was 120 mm. The matrices were made of SUS430 and the saturation magnetization was about 1.55 T.

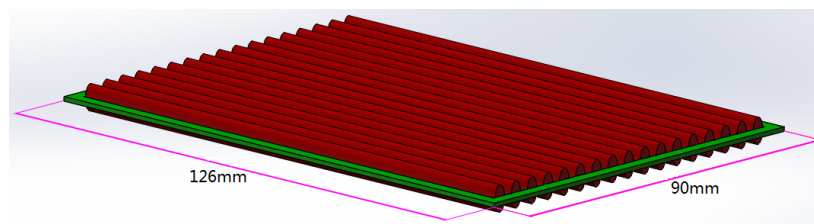


Fig. 3. A matrix unit

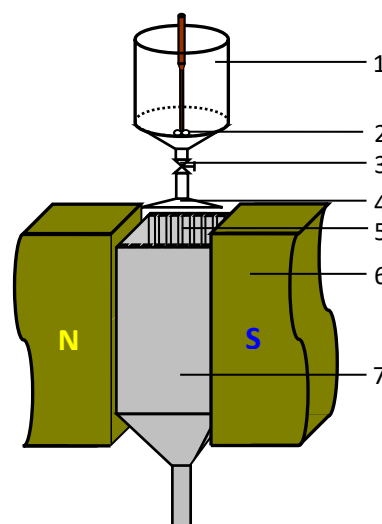


Fig. 4. Schematic diagram of the experimental apparatus: 1- container, 2- stirrer, 3- valve, 4- swinging feeder, 5- grooved channels, 6- magnetic pole, 7- tailored box

For the immobilization of the matrices, the matrices were firstly made into a matrix unit, as shown in Fig. 3. The matrices were welded on the nonmagnetic metal frame regularly. The total length and width of the matrix units were 126 mm and 90 mm, respectively. In a matrix unit, the matrices were

arranged along the direction of the short axis and the spacing between two adjacent matrices was 2mm. The short axis of the matrices was the same, so there were totally 17 matrices in a unit for all the three kinds of matrices.

Magnetic separation tests were conducted in a cyclic magnetic separator. The schematic diagram of the cyclic separator was shown in Fig. 4. The tailored box was used for the installation of the matrix units. The material of the box was nonmagnetic. The internal volume of the box was  $90 \times 72 \times 140 \text{ mm}^3$ . The inner wall of the box was grooved so that the matrix units could be inserted into the box through the grooved channels and fixed on it. This was different from the matrix installation in the transversal configuration wherein the matrix units were piled up layer by layer (Zheng et al., 2017d).

### 3.2. The sample

Pure hematite of two size fractions was used as the experimental sample:  $-25 \mu\text{m}$ ,  $25 \sim 38 \mu\text{m}$ . The Fe grade of the sample is about 68% and the purity is approximately 97%. The sample is purified from a hematite concentrate using shaking table. The magnetic susceptibility of the paramagnetic hematite is a constant and is about 0.0025.

### 3.3. Experimental methods

Fig. 5 showed the arrangement of the matrix units in the box. For the two kinds of elliptic matrices, two boxes with different channel distance were made. When installed in the boxes, the spacing between the matrix units  $m_1$  was 3mm. Then the distance of the units  $n_1$  for elliptic matrices of  $\lambda=1.6$  and  $\lambda=2$  were consequently 7.8 mm and 9 mm, respectively. So the channel distance in the box for the elliptic matrices of  $\lambda=1.6$  and  $\lambda=2$  were 7.8 mm and 9 mm, respectively. In this way, there were totally 9 units being installed in the box for the matrices of  $\lambda=1.6$  and 8 units for those of  $\lambda=2$ .

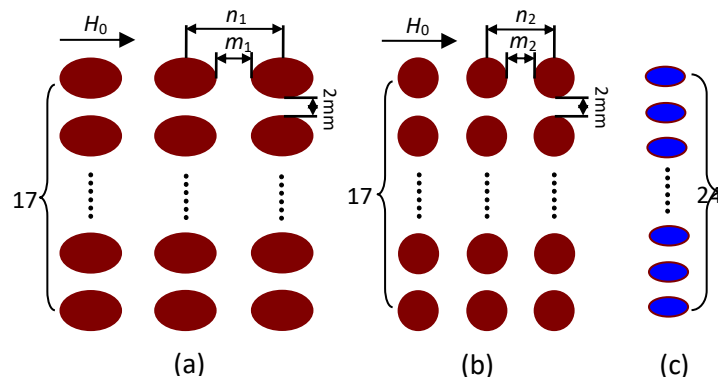


Fig. 5. Top view of the arrangement of the matrix units in the tailored box: (a) elliptic matrices of short axis equal to the diameter of the circular matrices; (b) the circular matrices; (c) elliptic matrices of long axis equal to the diameter of the circular matrices (to be considered)

For the comparison of the performance between circular and elliptic matrices, three schemes were considered: under the same unit number and unit distance ( $n_1=n_2$ ); under the same unit number and unit spacing ( $m_1=m_2$ ); under the condition that the unit spacing was equal ( $m_1=m_2$ ) and the circular matrix units were inserted in the box as more as possible, without ensuring the same unit number. The first scheme could be realized by just replacing the elliptic matrices with circular matrix in the respective boxes. For the latter two schemes, another box for circular matrices was made. The size of the box was the same as that of the former two. The distance between the channels was 6mm and a total of 12 channels could be grooved in the box. Thus a total of 12 circular matrix units were inserted in the box for the third scheme.

As shown in Fig. 5, the experimental process was the same as that in the transversal configuration (Zheng et al., 2017d). Briefly, the matrix units were firstly inserted into the tailored box through the grooved channels and the box was placed between the magnetic poles. 50g hematite particles and 450 ml were fully mixed in the container. After adjusting the applied magnetic field to a desired value, the

mixture was fed into the separation zone uniformly through the swinging feeder within about 20 s. The fluid velocity was about 0.1 m/s. After the feed process, the magnetic field was removed and the hematite particles captured by the matrices were flushed out and were dried and weighed. So the pulp density and the slurry velocity keep constant for all cycles. The recovery  $E$  was calculated with Eq. (13).

$$E = m_0 / 50 \times 100\% \quad (13)$$

where  $m_0$  was the mass of the hematite particles captured by the matrices. All experiments were conducted twice and the average values were adopted. The applied magnetic induction in the experimental process ranges from 0.1T~0.45T.

## 4. Results and discussion

### 4.1. Comparison of the recovery under the same unit number

Fig. 6 showed the capture efficiency of the circular matrices ( $\lambda=1$ ) and the elliptic matrices ( $\lambda=1.6$  and 2) under the same unit number. On the whole, the recovery increased with the increase of the particle size and the magnetic induction. According to the matrix unit arrangements in Fig. 5, the black and red lines were the recovery of the circular matrices under the same unit distance  $n_1$  and spacing  $m_1$  as that of the elliptic matrices, respectively. It could be seen that under the same unit distance ( $n_1=n_2$ ), the hematite recovery of the elliptic matrices was 5~20% higher than that of the circular matrices within the whole range of magnetic induction. Arranging circular matrices with the same unit spacing as that of elliptic matrices ( $m_1=m_2$ ), very limited increment of the recovery could be observed, the hematite recovery of the elliptic matrices was still much higher than that of the circular matrices in the whole range of applied magnetic induction.

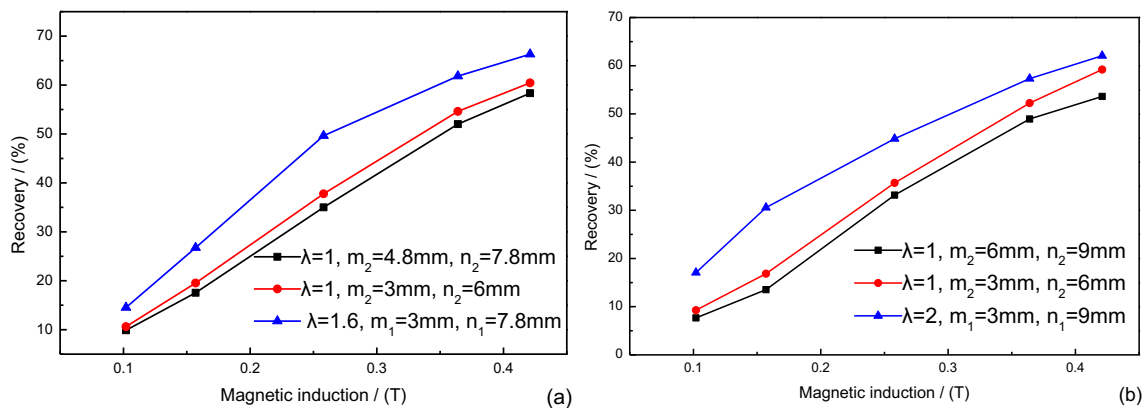


Fig. 6. Comparison of the hematite (-25  $\mu\text{m}$ ) recovery of the matrices under the same unit number: (a)  $\lambda=1, 1.6$  and unit number is 9; (b)  $\lambda=1, 2$  and unit number is 8

### 4.2. Comparison of the recovery when fully filled under the same unit spacing

With the same unit spacing of 3mm, the number of the matrices of  $\lambda=1, 1.6$  and 2 inserted into the boxes were 12, 9 and 8, respectively. As shown in Fig. 7, the same recovery regularity was observed for hematite particles of the two size fraction: the recovery increased with the increase of  $\lambda$  in low magnetic induction while decreased with the increase of  $\lambda$  in relatively high magnetic induction. The recovery difference between the circular and elliptic matrices was field dependent. This was different from the cases considered above.

The experimental results above showed different separation behaviors between the circular and elliptic matrices in the axial HGMS, which was determined by the particle capture behaviors of the matrices. Based on the expanded particle capture models above, the particle capture cross section of the matrices under a variety of circumstances were calculated and investigated, aiming at providing a theoretical support for the experimental experiments and revealing the key factors influencing the difference of the particle capture between the two kinds of matrices.

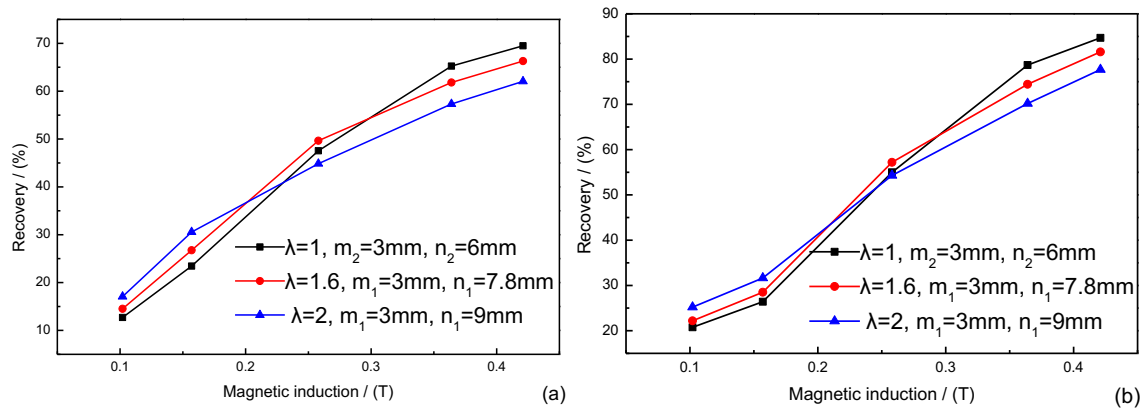


Fig. 7. Comparison of the recovery of the three kinds of matrices: (a)  $-25\ \mu\text{m}$ ; (b)  $25\sim 38\ \mu\text{m}$ , the unit number of the matrices of  $\lambda=1, 1.6$  and  $2$  were  $12, 9$  and  $8$ , respectively

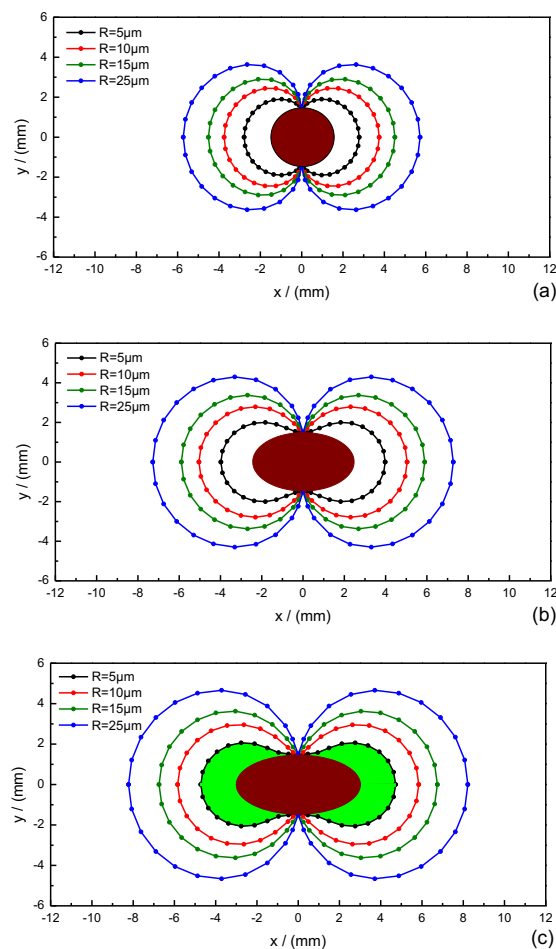


Fig. 8. Capture cross section of the hematite particles by the elliptic matrix of  $\lambda=1, 1.6$  and  $2$  under the applied magnetic induction of  $0.4\text{T}$

### 4.3. Analyses of experimental results with the particle capture cross section

#### 4.3.1. Analyses under the same unit number

For the calculation of the particle capture cross section, the following parameters were specified: The fluid velocity  $V_0=0.1\ \text{m/s}$  and the fluid viscosity  $\eta=1\ \text{mPa}\cdot\text{s}$ . The susceptibility of the hematite  $\kappa$  was  $0.0025$ . The matrix material was SUS430 and it was unsaturated until the applied magnetic field was above  $0.7\ \text{T}$ . Considering the experimental conditions, the particle capture cross section of the matrices

were investigated under the magnetic induction of 0.1 T, 0.2 T, 0.4 T and 0.8 T. Specially, the matrices were saturated in the magnetic induction of 0.8 T. Hematite particles of radius 5  $\mu\text{m}$ , 10  $\mu\text{m}$ , 15  $\mu\text{m}$  and 25  $\mu\text{m}$  were concerned.

Fig. 8 showed the particle capture cross section of the matrices of  $\lambda=1$ , 1.6 and 2 under the magnetic induction of 0.4 T. For all the matrices considered, the particle capture cross section became larger with the increase of the particle size and magnetic induction. This was ascribed to that the magnetic force acting on particles increased with the increase of the particle size and the magnetic induction. It could also be seen that the capture cross section of the elliptic matrix was larger than that of the circular matrix and that of matrix of  $\lambda=2$  was the largest. More particles could be captured by the elliptic matrices. Thus under the condition of the same matrix unit number, as shown in Fig. 6, the hematite recovery of the elliptic matrices was much higher than that of the circular matrices.

#### 4.3.2. Analyses when fully filled under the same unit spacing

When the tailored boxes were fully filled under the same unit spacing, as shown in Fig. 8, the hematite recovery of elliptic matrices was higher than that of circular matrices at low magnetic induction (0.10 T~0.21 T) but lower at relatively high magnetic induction (0.21 T~0.42 T). This could not be explained by that the elliptic matrix had larger capture cross section than the circular matrix as this was valid at both the magnetic field of 0.10 T and 0.42 T. For the explanation of this issue, it was necessary to quantify the particle capture cross section area. The capture cross section area was the area enclosed by the capture cross section boundary subtracted by the matrix area, as shown by the green region in Fig. 8(c). The capture cross section area could be calculated through the integration of the capture cross section boundary.

Fig. 9 showed the capture cross section area of the matrices as a function of magnetic induction. For all the particles considered, the capture cross section area of the matrix of  $\lambda=1$ , 1.6 and 2 increased successively. With increasing the magnetic field, the capture cross section area of all the matrices increased. However, the growth rate of the circular matrix ( $\lambda=1$ ) kept constant in the whole range of 0.1~0.8 T while the growth rate of the elliptic matrices decreased when magnetic induction exceeded 0.4 T.

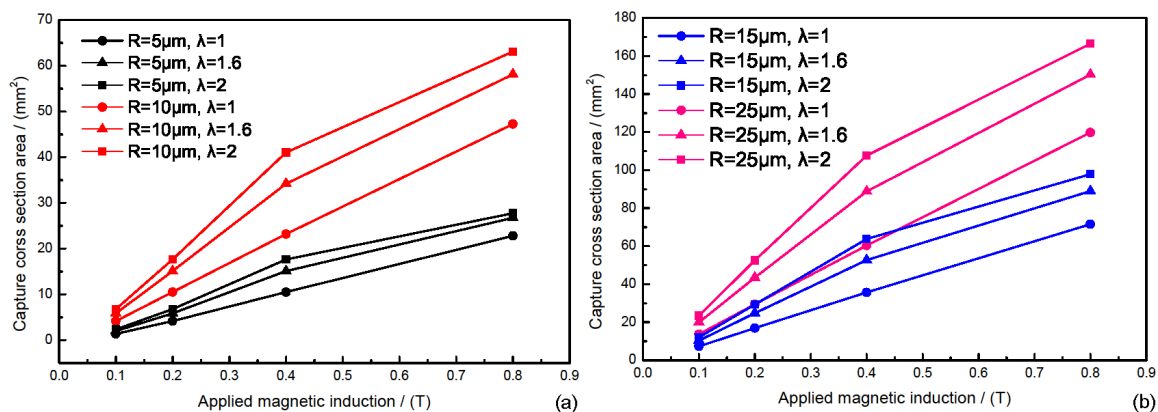


Fig. 9. Particle capture cross section area as a function of the applied magnetic field: (a)  $R=5 \mu\text{m}$  and  $10 \mu\text{m}$ ; (b)  $R=15 \mu\text{m}$  and  $25 \mu\text{m}$

Fig. 10 presented the capture cross section ratio of the elliptic matrix to circular matrix. The capture cross section area of the elliptic matrix was 1.4~1.8 times larger than that of the circular matrix within the induction of 0.1 T~0.4 T. When the induction exceeded 0.4 T, the ratio decreased rapidly. Under the induction of 0.1 T~0.2 T, for all the particles considered, the capture cross section area of the elliptic matrix of  $\lambda=1.6$  and 2 was about 1.4~1.5 and 1.7~1.8 times larger than that of the circular matrix respectively. That's why the hematite recovery of the elliptic matrices was higher than that of the circular matrices within the induction range of 0.10 T~0.21 T. Although the unit number of elliptic matrices was less than that of circular matrices, the total capture cross section area was still larger than

that of the circular matrices. The relation of the total capture cross section area:  $1.8 \times 8$  ( $\lambda=2$ )  $>$   $1.5 \times 9$  ( $\lambda=1.6$ )  $>$   $1 \times 12$  ( $\lambda=1$ ).

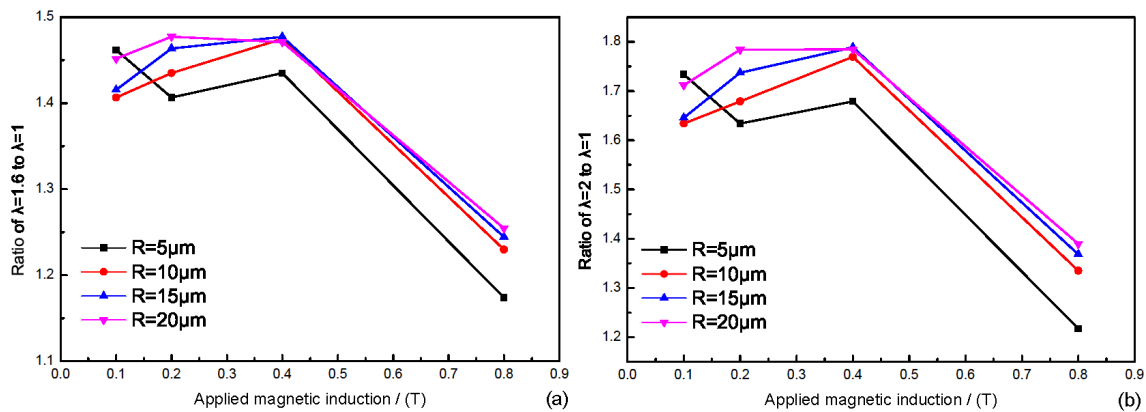


Fig. 10. Capture cross section ratio of elliptic matrix to circular matrix as a function of the applied magnetic field: (a) ratio of  $\lambda = 1.6$  to  $\lambda = 1$ ; (2) ratio of  $\lambda = 2$  to  $\lambda = 1$

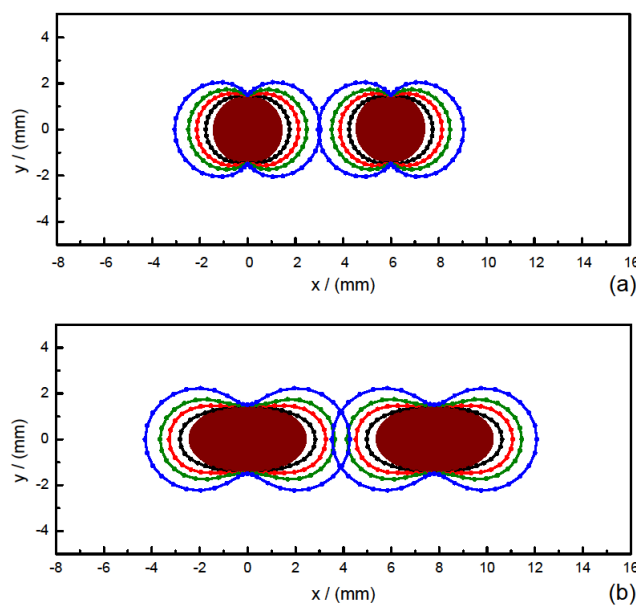


Fig. 11. Particle capture cross section of the circular and elliptic matrices at 0.1 T

However, the capture cross section area of elliptic matrix at 0.4 T was also 1.4~1.8 times larger than that of circular matrix, but the hematite recovery of the elliptic matrices was lower than that of the circular matrices, as shown in Fig. 7. This could be ascribed to the overlapping of the capture cross section, as shown in Figs. 11 and 12. Figs. 11 and 12 showed the capture cross section of the matrices under the magnetic induction of 0.1 T and 0.4 T, respectively. For both the circular and elliptic matrices in Fig. 11, very small part of the capture cross section overlapped. Thus the calculation of the cross section area was valid. But for the matrices in Fig. 12, most part of the capture cross section overlapped. The overlapping resulted in the invalidity of the calculated capture cross section area at 0.4T in Fig. 10. Although the overlapping occurred on circular and elliptic matrices, the overlapping reduced the difference of the capture cross section area between the two kinds of matrices, and consequently reduced the ratio. These reasons were responsible for the different capture behaviors of matrices at low and relatively high magnetic induction in Fig. 8. The overlapping of the capture cross section of matrices of  $\lambda=2$  was more significant than that of  $\lambda=1.6$ , resulting in the lowest recovery in relatively high magnetic induction.

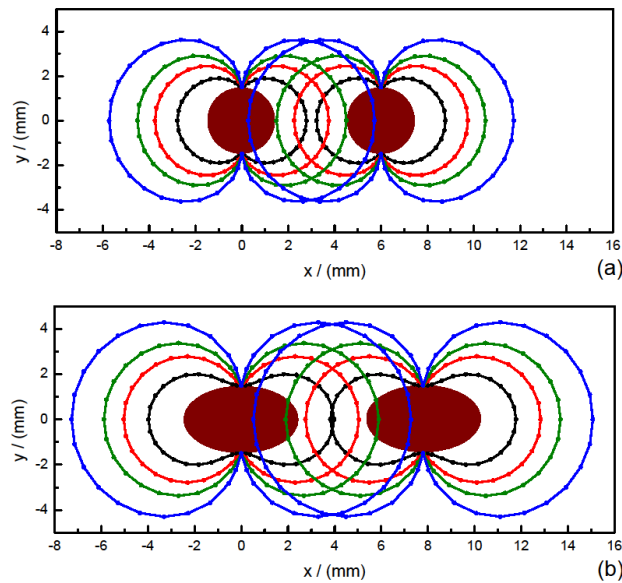


Fig. 12. Overlapping of the particle capture cross section of the circular and elliptic matrices at 0.4T

#### 4.3.3. Considerations for the application of elliptic matrices

When the separation space was fully filled with the same unit spacing, although the total number of elliptic matrices was much less than that of circular matrices, the hematite recovery of elliptic matrices could still be higher than that of circular matrices in relatively low magnetic induction due to the larger total particle capture cross section area. In fact, with the particle capture cross section ratio of elliptic matrix to circular matrix, the critical unit spacing under which the elliptic matrices had larger total capture cross section area without considering overlapping could be calculated with the following equation:

$$1 \times \frac{L}{2d+m} < \varepsilon \times \frac{L}{2\lambda d+m} \quad (14)$$

where  $L$  was the whole length for matrix inserting,  $\varepsilon$  was the particle capture cross section ratio of the two kinds of matrices,  $m$  was the unit spacing,  $d$  was the radius of the circular matrix. According to Fig. 10, for elliptic matrix of  $\lambda=1.6$  and 2, the corresponding  $\varepsilon$  was about 1.45 and 1.70, then the critical unit spacing  $m$  could be calculated. For elliptic matrix of  $\lambda=1.6$  and 2, the unit spacing should satisfy  $m > 0.67d$  and  $m > 0.86d$ , respectively. So the elliptic matrices had advantage over the circular matrix under large unit spacing and relatively low magnetic induction.

This study presented that the elliptic matrix had good magnetic characteristics. The overlapping of the particle capture cross section would decrease the difference of the two kinds of matrices and consequently decrease the superiority of elliptic matrix over circular matrix. For the substitution of circular matrices with elliptic matrices in axial HGMS, overlapping of the capture cross section of the target magnetic particles should be taken into consideration. The experimental and theoretical results also shed light on how to optimize the HGMS system with the elliptic matrices for improving the particle capture efficiency. As shown by Fig. 5(c), for the elliptic matrix with long axis equal to the diameter of circular matrix, a total of 24 matrices could be welded on the metal frame with the same adjacent spacing of 2mm. Under this circumstance, the overlapping of the particle capture cross section would be decreased. As the good magnetic characteristics of elliptic matrices, much better performance of elliptic matrices under this circumstance can be expected. This will be conducted experimentally and theoretically in our follow-up work, as well as the influence of some other process parameters such as the particle size, pulp density and slurry velocity.

## 5. Conclusions

In the present paper, three schemes were adopted to investigate the particle capture performance of matrices of  $\lambda = 1, 1.6$  and 2. Under the same matrix unit number, the elliptic matrices presented the

capture efficiency of 5~20% higher than that of the circular matrices and this was ascribed to the larger particle capture cross section area of elliptic matrices.

For the case that the separation space was fully filled under the same unit spacing, the capture efficiency of the elliptic matrices was higher than that of circular matrices in low magnetic field but lower in relatively high magnetic field. The higher capture efficiency in low magnetic field was ascribed to that the particle capture cross section area of the elliptic matrix was 1.4~1.8 times larger than that of the circular matrix and consequently the total capture cross section was larger, despite that the matrix unit number was less. Overlapping of the capture cross section in high magnetic field decreased the difference of the capture cross section area between circular and elliptic matrices, resulting in the lower capture efficiency of the elliptic matrices. The capture cross section area ratio of the elliptic matrix to circular matrix decreased rapidly at high magnetic field. For the substitution of circular matrices with elliptic matrices in axial HGMS, overlapping of the capture cross section of the target particles should be taken into consideration.

### Acknowledgments

This research work was financially supported by the National Natural Science Funds of China (Grant No. 51804341; No. 51674290), Natural Science Foundation of Hunan Province (Grant No. 2019JJ50833; No. 2016JJ3150), Innovation Driven Plan of Central South University (No. 2015CX005), Key Laboratory of Hunan Province for Calcium-containing Mineral Resources (No. 2018TP1002) and Co-Innovation Center for Clean and Efficient Utilization of Strategic Metal Mineral Resources.

### References

- ABBASOV, T., HERDEM, S., KÖKSAL, M., 1999. *Particle capture in axial magnetic filters with power law flow model*, J. Phys. D: Appl. Phys. 32, 1097-1103.
- ABBASOV, T., GÖGEBAKAN, V., KARADAĞ, T., 2016. *Particle capture modeling for an axial magnetic filter with a bounded non-Newtonian flow field*, Powder Technol. 291, 223-228.
- BRISS, R.R., GERBER, R., PARKER, M.R., 1976. *Theory and design of axially ordered filters for high intensity magnetic separation*, IEEE Trans. Magn. 12, 892-894.
- CHEN, H., BOCKENFELD, D., REMPFER, D., KAMINSKI, M.D., LIU, X., ROSENGART, A.J., 2008. *Preliminary 3-D analysis of a high gradient magnetic separator for biomedical applications*, J. Magn. Magn. Mater. 320, 279-284.
- CHEN, L., 2011. *Effect of magnetic field orientation on high gradient magnetic separation performance*, Miner. Eng. 24, 88-90.
- KANOK, H., MAYUREE, N., 2013. *The capture of micro-particles by random cylindrical wires in axial magnetic filters*, Sep. Sci. Technol. 48, 2234-2242.
- KIM, Y.G., SONG, J.B., YANG, D.G., LEE, J.S., PARK, Y.J., KANG, D.H., LEE, H.G., 2013. *Effects of filter shapes on the capture efficiency of a superconducting high-gradient magnetic separation system*, Supercond. Sci. Technol. 26, 85002-85008.
- LACOPA, Gh., REZLESCU, N., 1998. *Experimental observations on the saturation mass in the capture process of an ordered transverse high gradient magnetic separation matrix*, Powder Technol. 97, 233-236.
- LINDNER, J., MENZEL, K., NIRSCHL, H., 2013. *Parameters influencing magnetically enhanced centrifugal for protein separation*, Chemical Engineering Science, 97, 385-393.
- LI, W., HAN, Y., XU, R., GONG, E., 2018. *A preliminary investigation into separating performance and magnetic field characteristic analysis based on a novel matrix*, Minerals, 8, 1-16.
- LI, X.L., YAO, K.L., LIU, H.R., LIU, Z.L., 2007. *The investigation of capture behaviors of different shape magnetic sources in the high-gradient magnetic field*, J. Magn. Magn. Mater. 311, 481-488.
- MARIANI, G., FABBRI, M., NEGRINI, F., RIBANI, L., 2010. *High-Gradient Magnetic Separation of pollutant from wastewaters using permanent magnets*, Sep. Purif. Technol. 72, 147-155.
- NAKAI Y., MISHIMA F., AKIYAMA Y., NISHIJIMA S., 2010. *Development of high gradient magnetic separation system under dry condition*, Phys. C: Appl. Supercond. 470, 1812-1817.
- PASTEUR, A., TIPPKOTTER, N., KAMPEIS, P., ULBER, R., 2014. *Optimization of high gradient magnetic separation filter units for the purification of fermentation products*, IEEE Trans. Magn. 50 1-7.
- SINGH, V., NAG, S., TRIPATHY, S.K., 2013. *Particle flow modeling of dry induced roll magnetic separator*, Powder Technol. 244, 85-92.

- SINGH, S., SAHOO, H., RATH, S.S., SAHU, A.K., DAS, B., 2015. *Recovery of iron minerals from Indian iron ores slimes using colloidal magnetic coating*, Powder Technol. 269, 38-45.
- TOH, P.Y., YEAP, S.P., KONG, L.P., 2012. *Magnetophoretic removal of microalgae from fishpond water: Feasibility of high gradient and low gradient magnetic separation*, Chem. Eng. J. 211, 22-30.
- TRIPATHY, S.K., SURESH, N., 2017a. *Influence of particle size on dry high-intensity magnetic separation of paramagnetic mineral*, Adv. Powder Technol. 28, 1092-1102.
- TRIPATHY, S.K., SINGH, V., MURTHY, Y.R., Banerjee, P.K., SURESH, N., 2017b. *Influence of process parameters of dry high intensity magnetic separators on separation of hematite*, Int. J. Miner. Process. 160, 16-31.
- UCHIYAMA, S., KONDO, S., TAKAYASU, M., 1976. *Performance of parallel stream type magnetic filter for HGMS*, IEEE Trans. Magn. 12, 895-897.
- WANG, Y., DAN, X., ZHENG, X., LI, X., 2018a. *Study on the demarcation of applied magnetic induction for determining magnetization state of matrices in high gradient magnetic separation*, Miner. Eng. 127, 191-197.
- WANG, Y., DAN, X., ZHENG, X., LI, X., 2018b. *Rapid determination of the magnetization state of elliptic cross-section matrices for high gradient magnetic separation*, Powder Technol. 339, 139-148.
- WATSON, J.H.P., *Magnetic filtration*, 1973. J. Appl. Phys. 44, 4209-4213.
- WATSON, J.H.P., 1975, *Theory of capture of particles in magnetic high intensity filters*, IEEE Trans. Magn. 11, 1597-1599.
- ZHENG, X., WANG, Y., LU, D., 2015a. *Study on capture radius and efficiency of fine weakly magnetic minerals in high gradient magnetic field*, Miner. Eng. 74, 79-85.
- ZHENG, X., WANG, Y., LU, D., 2015b. *A realistic description of influence of the magnetic field strength on high gradient magnetic separation*, Miner. Eng. 79, 94-101.
- ZHENG, X., WANG, Y., LU, D., 2016a. *Investigation of the particle capture of elliptic cross-sectional matrix for high gradient magnetic separation*, Powder Technol. 297, 303-310.
- ZHENG, X., WANG, Y., LU, D., 2016b. *Effect of matrix shape on the capture of fine weakly magnetic minerals in high gradient magnetic separation*, IEEE Trans. Magn. 52, 7005111.
- ZHENG, X., WANG, Y., LU, D., 2016c. *Particle capture efficiency of elliptic cylinder matrices for high-gradient magnetic separation*, Sep. Sci. Technol. 51, 2090-2097.
- ZHENG, X., WANG, Y., LU, D., 2017a. *Study on buildup of fine weakly magnetic minerals on matrices in high gradient magnetic separation*, Physicochem. Probl. Miner. Process. 53(1), 94-109.
- ZHENG, X., GUO, N., CUI, R., LU, D., LI, X., LI, M., WANG, Y., 2017b. *Magnetic field simulation and experimental tests of special cross-sectional shape matrices for high gradient magnetic separation*, IEEE Trans. Magn. 53, 9200110.
- ZHENG, X., WANG, Y., LU, D., LI, X., LI, S., CHU, H., 2017c. *Comparative study on the performance of circular and elliptic cross-section matrices in axial high gradient magnetic separation: Role of the applied magnetic induction*, Miner. Eng. 110, 12-19.
- ZHENG, X., WANG, Y., LU, D., LI, X., 2017d. *Theoretical and experimental study on elliptic matrices in the transversal high gradient magnetic separation*, Miner. Eng. 111, 68-78.